LETTERS

Crystallographic preferred orientation of akimotoite and seismic anisotropy of Tonga slab

Rei Shiraishi[1], Eiji Ohtani[1], Kyuichi Kanagawa[3], Akira Shimojuku[1,4] & Dapeng Zhao[2]

The mineral akimotoite, ilmenite-structured $MgSiO_3$, exists at the bottom of the Earth's mantle transition zone and within the uppermost lower mantle, especially under low-temperature conditions[1]. Akimotoite is thought to be a major constituent of the harzburgite layer of subducting slabs, and the most anisotropic mineral in the mantle transition zone[2–4]. It has been predicted that if akimotoite crystals are preferentially oriented by plastic deformation, a cold subducted slab would be extremely anisotropic[5]. However, there have been no studies of crystallographic preferred orientations and very few reports of plastic deformation experiments for $MgSiO_3$ ilmenite. Here we present plastic deformation experiments on polycrystalline akimotoite, which were conducted at confining pressures of 20–22 GPa and temperatures of 1,000–1,300 °C. We found a change in crystallographic preferred orientation pattern of akimotoite with temperature, where the *c*-axis maximum parallel to the compression direction develops at high temperature, whereas the *c* axes are preferentially oriented parallel to the shear direction or perpendicular to the compression direction at lower temperature. The previously reported difference in compressional-wave seismic anisotropy between the northern and southern segments of the Tonga slab at depths of the mantle transition zone[6] can conceivably be attributed to the difference in the crystallographic preferred orientation pattern of akimotoite at varying temperature within the slab.

A polycrystalline akimotoite used for the present deformation experiments was synthesized at high pressure and temperature with a Kawai-type multi-anvil apparatus at Tohoku University. The synthesized polycrystalline akimotoite was confirmed to have no crystallographic preferred orientation (CPO).

The akimotoite specimen was then deformed by either uniaxial compression or simple shear geometry at high pressures and temperatures with the Kawai-type multi-anvil apparatus. The experimental conditions and results are given in Table 1.

We performed two types of experiment (types I and II; Table 1). In both type I and type II experiments, pressure was increased at room temperature, and temperature was then increased at the desired pressure. In type I experiments the sample was annealed for either 10 or 60 min, and then quenched. In type II experiments the sample was further deformed by slightly increasing the pressure, and then quenched. Two blank experiments were also conducted: a cold-compression experiment (DI01) and a non-annealing experiment (DI08). In run DI01, pressure was increased and then decompressed immediately. In run DI08, temperature was increased quickly (over about 10 min) to 1,200 °C after increasing the pressure, and the sample was subsequently quenched without annealing.

Recovered samples were cut in half parallel to the compression direction. Thin sections were then prepared and were polished with a colloidal silica suspension. A thin (~10 nm) coating of carbon was applied to decrease specimen charging. In each sample, the crystallographic orientations of 166–271 akimotoite grains were determined by the electron backscatter diffraction (EBSD) technique[7] (Table 1).

The change in sample thickness revealed the total compressional strains of samples deformed by uniaxial compression. The shear strain of specimen DI07 was calculated from the axial displacement of the pistons. The total compressional strains were 0.1–0.3. DI07 was deformed to a shear strain of 0.6. The microstructures and grain sizes (~10 μm) of samples, except specimen DI07, were similar. The grain size of DI07 was about 5 μm, slightly smaller than the other samples.

Equal-area lower-hemisphere projections of akimotoite $<11\bar{2}0>$, $<10\bar{1}0>$ and [0001] directions in the samples, deformed at 1,000–1,300 °C, are given in Fig. 1, where the compression and shear directions are shown by black arrows. Deformed polycrystalline $MgSiO_3$ akimotoite at 1,200–1,300 °C (Fig. 1a–c) has a CPO characterized by a strong *c*-axis maximum subparallel to the compression direction, and $<11\bar{2}0>$ and $<10\bar{1}0>$ axis girdles normal to the compression direction. This CPO suggests a dominant slip system with glide on (0001), which is in good agreement with the observation[8] that the dominant slip system in experimentally deformed akimotoite is 1/3 $<11\bar{2}0>$ (0001). In addition, the basal glide on (0001) was reported in some analogue of akimotoite, such as the trigonal structure of ilmenite[9]. In specimens deformed at 1,000 °C (Fig. 1d, e), the *c* axes

Table 1 | Summary of experimental conditions and results

Run no.	Pressure (GPa)	*P–T* path*	Assembly	Temperature (°C)	Heating duration (min)	Compressional strain	Shear strain	Grain size (μm)	CPO
DI01	21.1	–	Compression	–	–	0.16	–	7.4	Random
DI02	21.1	Type I	Compression	1,200	60	0.09	–	8.0	(0001) $\perp\sigma_1$
DI03	20.0→20.5	Type II	Compression	1,300	140	0.09	–	7.7	(0001) $\perp\sigma_1$
DI04	21.1	Type I	Compression	1,200	10	0.14	–	10.0	(0001) $\perp\sigma_1$
DI06	22.2→22.5	Type II	Compression	1,000	160	0.29	–	8.2	[0001] $\perp\sigma_1$
DI07	22.2	Type I	Shear	1,000	60	–	0.61	5.8	[0001] ||SD
DI08	21.1	–	Compression	1,200	0	0.14	–	8.0	Random

* We examined two types of pressure – temperature (*P–T*) path. In type I experiments, samples were annealed under the target conditions and then quenched. In type II experiments, the sample was further deformed by increasing the pressure slightly. $\perp\sigma_1$, perpendicular to the compression direction; \|\|SD, parallel to the shear direction.

[1]Institute of Mineralogy, Petrology, and Economic Geology. [2]Department of Geophysics, Tohoku University, Sendai 980-8578, Japan. [3]Department of Earth Sciences, Chiba University, Chiba 263-8522, Japan. [4]Department of Earth and Planetary Sciences, Faculty of Sciences, Kyushu University, Fukuoka 812-8581, Japan.

are preferentially orientated parallel to the shear direction or perpendicular to the compression direction. The CPO of the sample deformed in uniaxial compression is not axially symmetric, suggesting a deviation of its deformation from uniaxial geometry. The texture of the sample deformed in simple shear (DI07) is axially symmetric about the shear direction. Both $<11\bar{2}0>$ and $<10\bar{1}0>$ axes spread along a girdle around the *c*-axis maximum. This CPO therefore suggests the dominance of slip in the [0001] direction on multiple planes. In contrast, no clear CPO was developed in the sample deformed at room temperature (DI01) or in the non-annealing sample (DI08). From these blank tests, the CPOs observed in samples DI02–DI07 are considered to have developed during the plastic deformation at the target pressures and temperatures.

In addition, there is no difference in CPO pattern resulting from the difference between the *P*–*T* paths in the type I and type II experiments, judging from the fact that the CPO pattern of DI02 is the same as that of DI03.

Thus, observed akimotoite CPOs and inferred dominant slip systems differ in their deformation temperatures. Slip in the [0001] direction is probably dominant at a lower temperature (1,000 °C), whereas the basal glide on (0001) becomes dominant at higher temperatures (1,200–1,300 °C). The fabric transition occurs at about 1,100 °C. Fabric transitions with increasing temperature are also reported in other minerals such as quartz[10–12] and olivine[13–15]. For wet quartz it has been reported[16] that there is a possible transition from $<11\bar{2}0>$ (0001) to [0001]{$11\bar{2}0$} with increasing temperature. This observation is similar to that of akimotoite observed in this study.

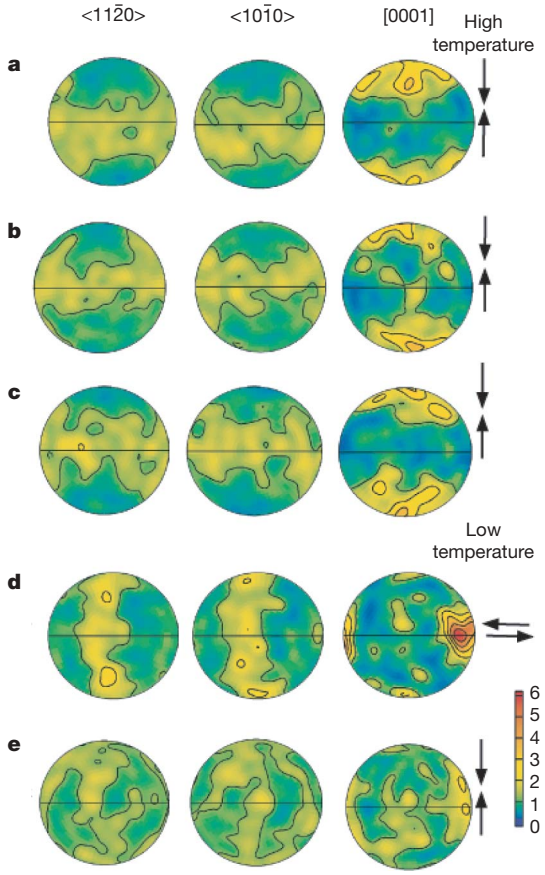

Figure 1 | Equal-area projections of pole figures for $<11\bar{2}0>$, $<10\bar{1}0>$ and [0001] directions of akimotoite in all samples. **a**, DI02 ($T = 1{,}200$ °C; $n = 271$); **b**, DI03 ($T = 1{,}300$ °C; $n = 197$); **c**, DI04 ($T = 1{,}200$ °C; $n = 220$); **d**, DI07 ($T = 1{,}000$ °C; $n = 166$); **e**, DI06 ($T = 1{,}000$ °C; $n = 216$); *n* is the number of grains measured. The projections are coloured according to the density of data points and are contoured at multiples of uniform distribution as shown in the scale at the bottom right. The north–south direction corresponds to the compression direction in **a**–**c** and **e**, and to the shear-plane normal direction in **d**. Pairs of bold arrows represent the compression direction or the shear direction.

We calculated seismic wave velocities from the akimotoite CPO data to examine the relationship between akimotoite CPO and seismic anisotropy. We used the elastic constants and density of akimotoite under the mantle transition zone conditions determined previously[4] with the molecular dynamic approach. The Voigt–Reuss–Hill average was used to calculate the seismic anisotropy. We used the program Anis2k (ref. 17) to calculate bulk elastic constants C_{ij} from the CPO data, as well as P-wave velocities. For the CPO data of DI03 and DI06 deformed in uniaxial compression, we randomly rotated the orientation data about the compression axis five times and used all rotated data for the following calculation, to decrease the deviations of those CPO data from uniaxial symmetry. Single-crystal akimotoite has a V_P anisotropy of 14.4%, which is shown in Fig. 2a. The results calculated from the CPO data for three representative samples (DI03, DI06 and DI07) are shown in Fig. 2b–d.

For the sample deformed at a higher temperature (DI03), the V_P anisotropy is 3.0%. In the sample deformed at a lower temperature, the V_P anisotropy of the compression experiment (DI06) and the simple shear experiment (DI07) are 1.0% and 4.3%, respectively. As regards other mantle transition-zone minerals, it has been reported[18] that the V_P anisotropies of 60% wadsleyite and 40% garnet deformed to shear strains of 1.0 and 0.5 are 2% and 1%, respectively. Although there are no CPO data for the other mantle transition-zone minerals, the anisotropy of a rock composed of 100% akimotoite is at least fourfold to fivefold that of a rock composed of 60% wadsleyite and 40% garnet. Akimotoite therefore has a much greater effect on the seismic anisotropy of subducting slabs at transition-zone depths.

Because of the difference in CPO pattern between the sample deformed at 1,300 °C (DI03) and that deformed at 1,000 °C (DI06 and DI07), the anisotropy pattern also depends on temperature. The P wave propagates most slowly in the shear direction or in the direction perpendicular to the compression direction at 1,000 °C, but in the compression direction at 1,300 °C. This is because the velocity of the P wave through an akimotoite single crystal is slowest in the *c*-axis direction (Fig. 2a).

The spatial variation of seismic anisotropy in the Tonga subducting slab was shown recently[6]. The slab is divided into two segments: the northern segment at latitudes 17–19° S and the southern segment at latitudes 19.5–27° S (Fig. 3). The magnitude of the anisotropy is 5–7% for P waves and 9–12% for S waves, and the direction of maximum velocity is different in each of the two slab segments. In the northern segment, P waves propagate more slowly in the slab normal direction. In contrast, P waves propagate more slowly in

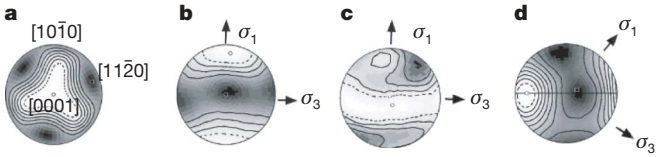

Figure 2 | P-wave anisotropies calculated using Anis2k. V_P contours are shown; black squares, maximum velocities (V_{max}); white circles, minimum velocities (V_{min}). **a**, Akimotoite single crystal. $V_{max} = 12.44$ km s^{-1}; $V_{min} = 10.77$ km s^{-1}. **b**, Akimotoite aggregate experimentally deformed at a relatively high temperature (1,300 °C) by uniaxial compression (DI03). $V_{max} = 11.65$ km s^{-1}; $V_{min} = 11.31$ km s^{-1}. **c**, **d**, Experimental deformation at a relatively low temperature (1,000 °C) by uniaxial compression (**c**; DI06; $V_{max} = 11.59$ km s^{-1}; $V_{min} = 11.47$ km s^{-1}) and by simple shear (**d**; DI07; $V_{max} = 11.67$ km s^{-1}; $V_{min} = 11.18$ km s^{-1}). The north–south direction corresponds to the compression direction in **b** and **c**, and to the shear-plane normal direction in **d**. The horizontal line and the east–west direction in **d** correspond to the shear plane and the shear direction, respectively. The σ_1 direction for the deformed samples is the direction of the advancing pistons.

the slab sinking direction in the southern segment. As regards S waves, the directions of maximum and minimum velocities do not coincide with the slab normal and sinking directions. We compared P-wave anisotropy in experimentally deformed akimotoite aggregates with that observed in the Tonga subducting slab as mentioned above (Figs 2 and 3). We assumed that the maximum compressive direction (σ_1) and the minimum compressive direction (σ_3) in experimentally deformed samples corresponded to the orientation of the principal stress axes estimated from focal mechanisms of deep earthquakes in the Tonga slab[6]. In the southern Tonga slab segment, the P-wave velocity is slower and faster in the σ_1 and σ_3 directions, respectively (Fig. 3c), which is similar to that in the akimotoite aggregate deformed at 1,300 °C (Fig. 2b). In contrast, in the northern Tonga slab segment, the P-wave velocity is faster in the σ_2 direction and slowest in the direction of the bisector between the σ_1 and σ_3 directions (Fig. 3b), which correlates well with that in the akimotoite aggregate deformed at 1,000 °C (Fig. 2d). Thus, the difference in seismic anisotropy between the northern and southern Tonga slab segments is attributable to the difference in CPO patterns of akimotoite resulting from differences in temperature. However, the transition temperature in the Tonga slab between the southern and northern segments could not be determined quantitatively because CPO patterns are also dependent on strain rate, and the geological strain rates are much smaller than the experimental strain rates. The geometry of the Tonga slab is complicated, specifically at greater depths[19,20] (Fig. 3). In addition, it has been reported that there is a difference in the distribution of the low-velocity zones in the mantle wedge between the northern and southern parts of the Tonga back-arc[21]. The low-velocity zone in the deep mantle wedge above the southern part of the Tonga slab may be caused by partial melting or by the existence of fluids from dehydration of the slab. These observations suggest that the temperature of the southern part of the Tonga slab is higher than that of the northern part. There are probably lateral variations in temperature in the Tonga slab that give rise to the difference in the seismic anisotropy pattern in the Tonga slab. It has been suggested that there are strong lateral variations in V_P and V_S, and that these variations are caused by a petrological anomaly, such as compositional or mineralogical variation[22]. In addition to compositional variation, the change in CPO pattern with temperature may have contributed to the differences between the northern and southern segments of the Tonga slab. Because ringwoodite and majorite, which may also be major constituents in the lower part of the mantle transition zone, are almost isotropic, the CPO of akimotoite must control the seismic anisotropy of the slab in the transition zone.

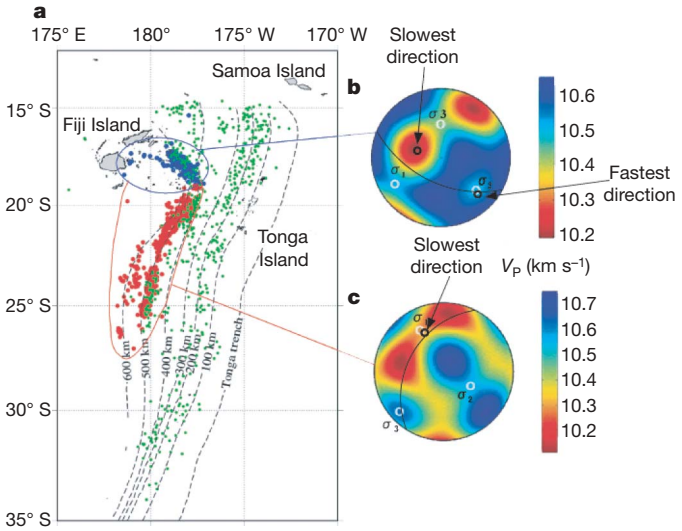

Figure 3 | P-wave anisotropy of the Tonga slab and the deformed akimotoite. a, Map showing the geometry of the subducting Tonga slab and epicentres of earthquakes. **b**, **c**, P-wave anisotropies of the northern (**b**) and southern (**c**) Tonga slab segments[6]. Green dots in **a** represent earthquake foci at depths between 100 and 500 km; blue and red dots show earthquakes at depths greater than 500 km in the northern and southern Tonga segments. The dashed lines are equal-depth contours of the Tonga slab[26]. The V_P contour diagrams (**b**, **c**) are equal-area lower-hemisphere projections, in which the white circles show the directions of the stress axes (σ_1, σ_2 and σ_3) in the Tonga slab deduced from the focal mechanism solutions, and the black arc lines show the intersection of the Tonga slab with the hemisphere at depths greater than 500 km. Black circles show the fastest and the slowest V_P directions expected from the deformed akimotoite.

METHODS SUMMARY

Experimental procedure. The furnace assembly was composed of a sintered ZrO_2 pressure medium (an octahedron with an edge length of 10 mm), Ta electrodes and a $LaCrO_3$ heater. Temperature was measured with W3%Re–W25%Re thermocouples. The starting material, which was placed in a platinum capsule, was an $MgSiO_3$ glass fabricated from oxides. Synthesis experiments were conducted at 20–22 GPa and 1,250–1,550 °C for 60 min.

We measured the water content of the starting material by Fourier-transform infrared spectroscopy with a JASCO MFT-2000 instrument. The water content was determined by integrating the infrared absorption spectrum from 3,200 to 3,750 cm^{-1} using a previous calibration of the extinction coefficient[23]. The water content in akimotoite is 24 p.p.m. by weight, which is extremely low compared with hydrous akimotoite[24].

The sample was sandwiched between hard alumina pistons inserted in the furnace assembly to produce differential stresses during compression. To minimize the deformation during cold compression, crushable alumina was placed at the outer ends of the pistons. Crushable alumina is initially very porous and soft. However, it becomes dense and works as good piston material on compression. These ideas and the cell assemblies were based on ref. 25.

EBSD measurement. EBSD patterns were obtained using a Nordlys II EBSD detector mounted on a Jeol JSM-6460 scanning electron microscope at Chiba University, operating with an accelerating voltage of 20 kV and a beam current of 1.5–2.4 nA, and indexed manually with Channel 5 software (Flamenco) from HKL Technology.

Received 23 October 2007; accepted 1 August 2008.

1. Akaogi, M., Tanaka, A. & Ito, E. Garnet–ilmenite–perovskite transitions in the system $Mg_4Si_4O_{12}$–$Mg_3Al_2Si_3O_{12}$ at high-pressures and high-temperatures: phase equilibria, calorimetry and implications for mantle structure. *Phys. Earth Planet. Inter.* **132,** 303–324 (2002).
2. Weidner, D. J. & Ito, E. Elasticity of $MgSiO_3$ in the ilmenite phase. *Phys. Earth Planet. Inter.* **40,** 65–70 (1985).
3. Da Silva, C. R. S., Karki, B. B., Stixrude, L. & Wentzcovitch, R. M. *Ab initio* study of the elastic behavior of $MgSiO_3$ ilmenite at high-pressure. *Geophys. Res. Lett.* **26,** 943–946 (1999).
4. Zhang, Y., Zhao, D. & Matsui, M. Anisotropy of akimotoite: A molecular dynamics study. *Phys. Earth Planet. Inter.* **151,** 309–319 (2005).
5. Anderson, D. L. *Theory of the Earth* (Blackwell, 1989).
6. Vavryčuk, V. Spatially dependent seismic anisotropy in the Tonga subduction zone: A possible contributor to the complexity of deep earthquakes. *Phys. Earth Planet. Inter.* **155,** 63–72 (2006).
7. Randle, V. *Microtexture Determination and its Applications* 2nd edn (Maney, 2003).
8. Cordier, P. in *Plastic Deformation of Minerals and Rocks* (eds Karato, S. I. & Wenk, H. R.) 137–179 (American Mineralogical Society, 2002).
9. Bascou, J., Raposo, M. I. B., Vauchez, A. & Egydio-Silva, M. Titanohematite lattice-preferred orientation and magnetic anisotropy in high-temperature mylonites. *Earth Planet. Sci. Lett.* **198,** 77–92 (2002).
10. Lister, G. S. Fabric transitions in plastically deformed quartzites: competition between basal, prism and rhomb systems. *Bull. Mineral.* **102,** 232–241 (1979).
11. Schmid, S. M. & Casey, M. Complete fabric analysis of some commonly observed quartz *c*-axis patterns. *Am. Geophys. Un. Geophys. Monogr.* **36,** 263–286 (1986).
12. Mainprice, D., Bouchez, J.-L., Blumenfeld, P. & Tubia, J. M. Dominant *c* slip in naturally deformed quartz; implications for dramatic plastic softening at high temperature. *Geology* **14,** 2181–2202 (1986).
13. Katayama, I. & Karato, S. Effect of temperature on the B- to C-type olivine fabric transition and implication for flow pattern in subduction zones. *Phys. Earth Planet. Inter.* **157,** 33–45 (2006).
14. Carter, N. L. & Ave'Lallemant, H. G. High temperature flow of dunite and peridotite. *Geol. Soc. Am. Bull.* **81,** 2181–2202 (1970).
15. Jung, H. & Karato, S.-I. Water-induced fabric transitions in olivine. *Science* **293,** 1460–1463 (2001).
16. Blacic, J. D. Plastic deformation mechanisms in quartz: The effect of water. *Tectonophysics* **27,** 271–294 (1975).
17. Mainprice, D. A. FORTRAN program to calculate seismic anisotropy from the lattice preferred orientation of minerals. *Comput. Geosci.* **16,** 385–393 (1990).

18. Tommasi, A., Mainprice, D., Cordier, P., Thoraval, C. & Couvy, H. Strain-induced seismic anisotropy of wadsleyite polycrystals and flow patterns in the mantle transition zone. *J. Geophys. Res.* **109,** B12406, doi:10.1029/2005JB004168 (2004).
19. Chen, W.-P. & Brudzinski, M. R. Evidence for a large-scale remnant of subducted lithosphere beneath Fiji. *Science* **292,** 2475–2479 (2001).
20. Chen, W.-P. & Brudzinski, M. R. Seismic anisotropy in the mantle transition zone beneath Fiji–Tonga. *Geophys. Res. Lett.* **30,** 1682, doi:10.1029/2002GL016330 (2003).
21. Zhao, D. *et al.* Depth extent of the Lau back-arc spreading center and its relation to subduction processes. *Science* **278,** 254–257 (1997).
22. Brudzinski, M. R. & Chen, W.-P. A petrologic anomaly accompanying outboard earthquakes beneath Fiji–Tonga: Corresponding evidence from broadband P and S waveforms. *J. Geophys. Res.* **108,** B62299, doi:10.1029/2002JB002012 (2003).
23. Paterson, M. S. The determination of hydroxyl by infrared absorption in quartz, silicate glasses and similar materials. *Bull. Mineral.* **105,** 20–29 (1982).
24. Bolfan-Casanova, N., Keppler, H. & Rubie, D. C. Water partitioning between nominally anhydrous minerals in the $MgO–SiO_2–H_2O$ system up to 24 GPa: implications for the distribution of water in the Earth's mantle. *Earth Planet. Sci. Lett.* **182,** 209–221 (2000).
25. Karato, S. & Rubie, D. C. Toward an experimental study of deep mantle rheology: A new multianvil sample assembly for deformation studies under high pressures and temperatures. *J. Geophys. Res.* **102,** 20111–20122 (1997).
26. Gudmundsson, O. & Sambridge, M. A regionalized upper mantle (RUM) seismic model. *J. Geophys. Res.* **103,** 7121–7136 (1998).

Acknowledgements This work was supported by a Grant-in-Aid for Scientific Research from the Ministry of Education, Culture, Science, Sport, and Technology of the Japanese Government.

Author Contributions R.S. performed experiments and took the lead in writing the manuscript. E.O. and A.S. designed the study. K.K. performed EBSD analyses. D.Z. worked on the seismological aspects of this study. All co-authors took part in the discussion and interpretation of the results and improving the manuscript.

Author Information Reprints and permissions information is available at www.nature.com/reprints. Correspondence and requests for materials should be addressed to R.S. (siraisir@ganko.tohoku.ac.jp).